

This is an Open Access document downloaded from ORCA, Cardiff University's institutional repository: <https://orca.cardiff.ac.uk/id/eprint/117569/>

This is the author's version of a work that was submitted to / accepted for publication.

Citation for final published version:

Beltrachini, Leandro 2018. A finite element solution of the forward problem in EEG for multipolar sources. IEEE Transactions on Neural Systems and Rehabilitation Engineering 27 (3) , pp. 368-377. 10.1109/TNSRE.2018.2886638

Publishers page: <http://dx.doi.org/10.1109/TNSRE.2018.2886638>

Please note:

Changes made as a result of publishing processes such as copy-editing, formatting and page numbers may not be reflected in this version. For the definitive version of this publication, please refer to the published source. You are advised to consult the publisher's version if you wish to cite this paper.

This version is being made available in accordance with publisher policies. See <http://orca.cf.ac.uk/policies.html> for usage policies. Copyright and moral rights for publications made available in ORCA are retained by the copyright holders.



A finite element solution of the forward problem in EEG for multipolar sources

L. Beltrachini

Abstract—Multipolar source models have been presented in the context of electro/magnetoencephalography (E/MEG) to compensate for the limitations of the classical equivalent current dipole to represent realistic generators of brain activity. Although there exist several reports accounting for the advantages of multipolar components over single dipoles, there is still no available numerical implementation in fully-personalised scenarios. In this paper, we present, for the first time, a finite element framework for simulating EEG signals generated by multipolar current sources in individualised, heterogeneous, and anisotropic head models. This formulation is based on the subtraction approach, guaranteeing the existence and uniqueness of the solution. In particular, we analyse the cases of monopolar, dipolar, and quadrupolar source components, for which we study their performance in idealised and realistic head models. Numerical solutions are compared with analytical formulas in multi-layered spherical models. Such formulas are available in the case of monopolar and dipolar sources, and here derived for the quadrupolar components. We finally illustrate their advantages in the description of extended current generators using a realistic head model. The framework presented here enables further analysis towards the estimation of biophysically-principled source parameters from standard E/MEG experiments.

Index Terms— EEG, forward problem, extended sources, subtraction approach, finite element method

I. INTRODUCTION

Electromagnetic source models play a significant role in the characterisation of generators of brain activity by means of electro/magnetoencephalography (E/MEG). Few years after the first EEG signals were acquired in humans [1], Adrian and Matthews [2] suggested that dipole-like current generators may be responsible for such measurements. This suggestion was later considered by Shaw and Roth [3] for presenting, for the first time, the mathematical dipole model. Since then, numerous studies confirmed the dipolar source model as appropriate for representing signal generators at different length scales, ranging from small columns [4] to extended regions [5]. This made the dipolar representation a standard assumption in E/MEG source analysis [6], [7].

It was not until the mid 1990's that researchers started to question the validity of the equivalent dipolar source model for representing current generators in the brain. First, the equivalent dipole was shown to introduce significant errors for describing extended sources of electrical activity as seen by

MEG [8]–[10]. Such macroscopic sources (i.e. in the spatial scale ranging from single brain areas to the entire brain; larger than 6.25 mm^2) were reported in evoked potentials (in the range $40\text{--}400 \text{ mm}^2$ [11]) and epilepsy (in the range $400\text{--}2000 \text{ mm}^2$ [12]), and therefore of primary clinical importance. More recently, both theoretical [13] and experimental [14] evidence have shown the limitations of the dipolar model for representing sources in the mesoscale (i.e. in the spatial scale ranging from an anatomic microcolumn to a group of functional columns; between $30\text{--}2500 \mu\text{m}$). Source models in such scale represent the minimum unit responsible for the generation of measurable EEG activity, and are therefore fundamental for estimating biophysical parameters from electrophysiological recordings such as scalp and intracranial EEG [15] (see Section IV).

As a response to the reported inaccuracies of the equivalent dipole model, several alternatives started to emerge. Between them, the multipolar expansion stood out for its rigour and flexibility to represent arbitrary source distributions. This approach consists in approximating the field produced by an extended source by several terms of the corresponding Taylor series expansion around its centroid [16]. If only the first symmetric term is considered, the approximation leads to the equivalent dipolar source. As a consequence, the multipolar expansion can be seen as the natural generalisation of the equivalent dipole model. In fact, the inclusion of higher order terms in the aforementioned expansion has led to improvements in field representations. In the case of MEG, the addition of quadrupolar components allowed to reduce the errors in source localisation considerably [10]. Similarly, the utilisation of multipolar components has been shown necessary for describing mesoscopic sources accurately based on invasive EEG recordings [14].

Notwithstanding the evidence supporting the utilisation of multipolar source models, there is still no numerical framework allowing their use in fully-realistic scenarios. Existing simulations were based on simplistic head and tissue representations, such as single-shell spheres [10], [17], [18] or assuming isotropic and homogeneous conductivity fields [14]. This prevents the full exploitation of multipolar components for accurate description of E/MEG signals, for which realistic and individualised tissue and head models are needed [19]–[21]. The availability of a flexible tool would allow to get insights into the characterisation of the generators of brain activity via *in silico* experiments (e.g. for studying the sensitivity of the acquisition methodology to such generators) as well as based on real data, whose analysis relies on the computation

L. Beltrachini is with the Cardiff University Brain Research Imaging Centre (CUBRIC), School of Physics and Astronomy, Cardiff University, Cardiff CF24 4HQ, UK. (email: BeltrachiniL@cardiff.ac.uk).

of predefined solutions (i.e. the lead-field matrix).

In this paper, we present a full subtraction version of the finite element method (FEM) for solving the forward problem in EEG (EEG-FP) considering multipolar sources in personalised head models. We extend the formulation presented by Drechsler *et al.* [22] for dealing with monopolar and quadrupolar components, in addition to dipoles. This makes the presented method the first allowing to simulate such sources in anisotropic and non-spherical domains. The adoption of the subtraction technique allows to guarantee the existence and uniqueness of the solution for symmetric source configurations. Results of the EEG-FP utilising a multi-layered spherical domain were compared with the corresponding analytical solutions, which we generalised for multipolar source models. Finally, we illustrate their use in a realistic head model, and show the impact of multipolar source models on the characterisation of extended sources. The tools developed here were fully implemented in MATLAB R2015a (The MathWorks Inc., Natick, MA), and are publicly accessible through the FEMEG toolbox (<https://femeg.github.io>).

II. METHODS

A. Forward problem

The EEG-FP consists in finding the electric potential function $u(\mathbf{r})$ due to a current source with density $s(\mathbf{r})$ defined over the domain Ω (i.e. the head), with boundary Γ . Let $\bar{\boldsymbol{\sigma}}(\mathbf{r})$ be the rank-2 conductivity tensor field within Ω , and $\hat{\mathbf{n}}(\mathbf{r})$ the unitary vector normal to Γ (pointing outwards). Then, under generally accepted assumptions (as the *quasistatic* and the *point electrode model* approximations), the EEG-FP reduces to find $u(\mathbf{r})$ satisfying [23]

$$\begin{cases} \nabla \cdot (\bar{\boldsymbol{\sigma}}(\mathbf{r}) \nabla u(\mathbf{r})) = -s(\mathbf{r}), & (\mathbf{r} \in \Omega), \\ \langle \bar{\boldsymbol{\sigma}}(\mathbf{r}) \nabla u(\mathbf{r}), \hat{\mathbf{n}}(\mathbf{r}) \rangle = g(\mathbf{r}), & (\mathbf{r} \in \Gamma), \end{cases} \quad (1)$$

where $g(\mathbf{r})$ is an arbitrary function fulfilling [24]

$$\int_{\Omega} s(\mathbf{r}) d\mathbf{r} = - \int_{\Gamma} g(\mathbf{r}) d\mathbf{r}. \quad (2)$$

It is clear from (1) that the source density function plays a key role in the solution of the EEG-FP. Accurate source models are then of paramount importance for characterising generators of electrical activity based on potential recordings reliably. In the following, we introduce the multipolar expansion technique as a method to describe arbitrary sources with great level of detail.

B. The multipolar expansion

Let Ω_f be the source domain (in any arbitrary spatial scale) and $f(\mathbf{r}_f, \mathbf{r})$ the electric potential in \mathbf{r} outside Ω_f due to a unitary current source located in $\mathbf{r}_f = \mathbf{r}_o + \mathbf{a}$, $\mathbf{r}_f \in \Omega_f$, with \mathbf{r}_o being an arbitrary point. Then, we expand f about \mathbf{r}_o in Taylor series, yielding

$$\begin{aligned} f(\mathbf{r}_o + \mathbf{a}, \mathbf{r}) &= f(\mathbf{r}_o, \mathbf{r}) + \mathbf{a} \cdot \nabla_o f(\mathbf{r}_o, \mathbf{r}) \\ &+ \frac{1}{2} \mathbf{a}^T \nabla_o (\nabla_o f(\mathbf{r}_o, \mathbf{r})) \mathbf{a} + \dots \end{aligned} \quad (3)$$

This series expansion converges provided that $\|\mathbf{a}\| < \|\mathbf{r} - \mathbf{r}_o\|$, for all $\mathbf{r}_f \in \Omega_f$ [16, p. 178]. The potential in \mathbf{r} due to the entire source is then

$$\begin{aligned} u(\mathbf{r}) &= \int_{\Omega_f} f(\mathbf{r}_f, \mathbf{r}) s(\mathbf{r}_f) d\mathbf{r}_f = q f(\mathbf{r}_o, \mathbf{r}) + \mathbf{q} \cdot \nabla_o f(\mathbf{r}_o, \mathbf{r}) \\ &+ \frac{1}{2} \mathbf{Q} : \nabla_o (\nabla_o f(\mathbf{r}_o, \mathbf{r})) + \dots, \end{aligned} \quad (4)$$

where

$$q = \int_{\Omega_f} s(\mathbf{r}_f) d\mathbf{r}_f, \quad (5)$$

$$\mathbf{q} = \int_{\Omega_f} (\mathbf{r}_f - \mathbf{r}_o) s(\mathbf{r}_f) d\mathbf{r}_f, \quad (6)$$

$$\mathbf{Q} = \int_{\Omega_f} (\mathbf{r}_f - \mathbf{r}_o)(\mathbf{r}_f - \mathbf{r}_o)^T s(\mathbf{r}_f) d\mathbf{r}_f, \quad (7)$$

are the monopolar, dipolar, and quadrupolar components of $s(\mathbf{r})$, respectively, and we used the identity $\mathbf{a}^T \nabla_o (\nabla_o f(\mathbf{r}_o)) \mathbf{a} = (\mathbf{a} \mathbf{a}^T) : \nabla_o (\nabla_o f(\mathbf{r}_o))$, with $:$ being the tensor contraction [18].

Based on (4), it is possible to define source density functions representing each term individually. In case of employing $s(\mathbf{r}) = q \delta(\mathbf{r} - \mathbf{r}_o)$, the monopolar term is the only different from zero. For this reason, we call it the equivalent monopolar source term model, or simply a monopole. The electric potential generated by this source is then obtained by solving (1) with $g(\mathbf{r}) = -A^{-1}$, where A is the area of Γ . Similarly, we can represent a dipolar source by setting $s(\mathbf{r}) = -\mathbf{q} \cdot \nabla \delta(\mathbf{r} - \mathbf{r}_o)$. This can be further verified by applying the operator $\mathbf{q} \cdot \nabla_o (\cdot)$ to both terms in (1) assuming a unitary monopolar source, and noting that $\nabla_o \delta(\mathbf{r} - \mathbf{r}_o) = -\nabla \delta(\mathbf{r} - \mathbf{r}_o)$. Finally, a purely quadrupolar source is obtained if $s(\mathbf{r}) = \frac{1}{2} \mathbf{Q} : \nabla (\nabla (\delta(\mathbf{r} - \mathbf{r}_o)))$, which can be verified by applying the operator $\frac{1}{2} \mathbf{Q} : \nabla_o (\nabla_o (\cdot))$ to both terms in (1) for a unitary monopole. In these cases, the electric potential satisfies (1) with $g(\mathbf{r}) = 0$. It is worth noting that these expressions are valid for generalised functions only and not in a classical sense.

Many authors find it convenient to write $s(\mathbf{r})$ in terms of the current density vector representing the synchronous activity of a local neuronal population, generally called *principal* or *impressed current density vector*, and denoted $\mathbf{J}^p(\mathbf{r})$. The relation is given by $s(\mathbf{r}) = -\nabla \cdot \mathbf{J}^p(\mathbf{r})$ [25, Secs. 7.2.2 and 8.5]. This gives the classical result for dipolar sources, where the principal current density vector is $\mathbf{J}^p(\mathbf{r}) = \mathbf{q} \delta(\mathbf{r} - \mathbf{r}_o)$. In the case of a quadrupolar source, the impressed current turns out to be $\mathbf{J}^p(\mathbf{r}) = \frac{1}{2} \mathbf{Q} \nabla \delta(\mathbf{r} - \mathbf{r}_o)$.

From the previous analysis, it can be noted that the multipolar expansion is a clear extension to the classical dipolar source model. The inclusion of multipolar terms other than the dipole allows a finer representation of current sources across multiple scales: at a mesoscopic level, these extra components enable to consider more complex spatial arrangements of *sources and sinks* [13], [14]; at a macroscopic level, they allow a much finer representation of electro-physiological recordings due to extended sources at very little expense (five parameters for a quadrupole) [10].

C. Finite element formulation

1) *Subtraction approach*: To obtain a proper discretisation of (1) using the FEM it is convenient to avoid the singularity in the source term (which may also prevent to perform the integration by parts needed in standard FEM). The most common way to solve this problem is known as the *subtraction approach* [22], [23], [26]. It consists in splitting the electric potential due to a point-like source located in \mathbf{r}_o in two terms, one representing the potential due to the source in an infinite, homogeneous space (for which analytical formulas are used), and the other acting as a *correction potential* due to the heterogeneity and finiteness of the domain. This is done by finding a non-empty subdomain $\Omega^\infty \subseteq \Omega$ centred in \mathbf{r}_o with homogeneous electrical conductivity $\bar{\sigma}(\mathbf{r}_o) = \bar{\sigma}^\infty$. The electrical conductivity field is then expressed as $\bar{\sigma}(\mathbf{r}) = \bar{\sigma}^\infty + \bar{\sigma}^c(\mathbf{r})$, where $\bar{\sigma}^c(\mathbf{r})$ is the correction conductivity tensor, and satisfies $\bar{\sigma}^c(\mathbf{r}) = \mathbf{0}, \forall \mathbf{r} \in \Omega^\infty$. This allows to split the electric potential function in two parts, $u(\mathbf{r}) = u^\infty(\mathbf{r}) + u^c(\mathbf{r})$, where $u^\infty(\mathbf{r})$ and $u^c(\mathbf{r})$ are the singularity and correction potentials, respectively.

The singularity potential is defined as the potential due to a multipolar source in an unbounded homogeneous domain with electrical conductivity $\bar{\sigma}^\infty$. Analytical expressions can be easily obtained for $u^\infty(\mathbf{r})$ when considering isotropic conductivity in Ω^∞ , i.e. $\bar{\sigma}^\infty = \sigma^\infty \mathbf{I}_3$, with \mathbf{I}_n being the $n \times n$ identity matrix. In this case, the singularity potential is found by solving $\Delta u^\infty(\mathbf{r}) = -s(\mathbf{r})/\sigma^\infty$. The solutions for monopolar, dipolar, and quadrupolar sources are, respectively,

$$u_m^\infty(\mathbf{r}) = \frac{1}{4\pi\sigma^\infty} \frac{q}{R}, \quad (8)$$

$$u_q^\infty(\mathbf{r}) = \frac{1}{4\pi\sigma^\infty} \frac{\mathbf{q} \cdot \mathbf{R}}{R^3}, \quad (9)$$

$$u_Q^\infty(\mathbf{r}) = \frac{1}{4\pi\sigma^\infty} \frac{\mathbf{Q}}{2} : \frac{R^2 \mathbf{I}_3 - 3\mathbf{R}\mathbf{R}^T}{R^5}, \quad (10)$$

with $\mathbf{R} = \mathbf{r} - \mathbf{r}_o$ and $R = |\mathbf{R}|$.

Then, the problem turns to find the correction term. Based on the previous definitions, it is straightforward to show that $u^c(\mathbf{r})$ satisfies

$$\begin{cases} \nabla \cdot (\bar{\sigma}(\mathbf{r}) \nabla u^c(\mathbf{r})) = -f(\mathbf{r}), & (\mathbf{r} \in \Omega) \\ \langle \bar{\sigma}(\mathbf{r}) \nabla u^c(\mathbf{r}), \hat{\mathbf{n}}(\mathbf{r}) \rangle = h(\mathbf{r}), & (\mathbf{r} \in \partial\Omega) \end{cases}, \quad (11)$$

where $f(\mathbf{r}) = \nabla \cdot (\bar{\sigma}^c(\mathbf{r}) \nabla u^\infty(\mathbf{r}))$ and $h(\mathbf{r}) = g(\mathbf{r}) - \langle \bar{\sigma}(\mathbf{r}) \nabla u^\infty(\mathbf{r}), \hat{\mathbf{n}}(\mathbf{r}) \rangle$. This formulation is the one needing a numerical discretisation by the FEM.

In the following, we assume symmetric source components, for which $g = 0$ in (1). This condition, usually known as the *source conservation principle in resistive media*, is fulfilled by sets of dipoles, quadrupoles, and monopoles with net density equal to zero, and avoids currents flowing out of Ω .

2) *Full subtraction FEM*: To approximate the solution of the EEG-FP with the FEM, we first need to find the variational formulation of the subtraction version. This is obtained by multiplying the differential equation in (11) by a test function v belonging to a suitable space H , and then integrating over the domain [26]. After employing the divergence theorem and the boundary condition, the variational formulation results in finding $u^c(\mathbf{r}) \in H$ such that, for all $v(\mathbf{r}) \in H$, satisfies

$a(u^c, v) = l(v)$, where $a : H \times H \rightarrow \mathbb{R}$ is the bilinear form given by

$$a(u, v) = \int_{\Omega} \langle \bar{\sigma}(\mathbf{r}) \nabla u(\mathbf{r}), \nabla v(\mathbf{r}) \rangle d\mathbf{r}, \quad (12)$$

and $l : H \rightarrow \mathbb{R}$ is the linear form defined as

$$l(v) = - \int_{\Omega} \langle \bar{\sigma}^c(\mathbf{r}) \nabla u^\infty(\mathbf{r}), \nabla v(\mathbf{r}) \rangle d\mathbf{r} - \int_{\Gamma} v(\mathbf{r}) \langle \bar{\sigma}^\infty \nabla u^\infty(\mathbf{r}), \hat{\mathbf{n}}(\mathbf{r}) \rangle d\mathbf{r}. \quad (13)$$

The following step consists in discretising Ω into a set of *finite elements*. Such tessellation is used to construct a discretised space $V_N \subset H$ where to find the numerical solution. As is usual in the field, we choose $V_N = \text{span}\{\varphi_i(\mathbf{r}) : i = 1, \dots, N\}$, with $\varphi_i(\mathbf{r})$ being piecewise functions satisfying $\varphi_i(\mathbf{p}_j) = \delta_{ij}$, and N the number of nodes [26]. Then, we look for $\tilde{u}^c(\mathbf{r}) \in V_N$ (an approximation of $u^c(\mathbf{r}) \in H$) satisfying $a(\tilde{u}^c, v) = l(v)$ for all $v(\mathbf{r}) \in V_N$. This leads to solve the linear system

$$\mathbf{K} \mathbf{u}^c = \mathbf{b}, \quad (14)$$

where $\mathbf{K} \in \mathbb{R}^{N \times N}$ is the *stiffness matrix* defined by $K_{ij} = a(\varphi_i(\mathbf{r}), \varphi_j(\mathbf{r}))$, $\mathbf{b} \in \mathbb{R}^N$ is the *source vector* with elements $b_i = l(\varphi_i(\mathbf{r}))$, and $\mathbf{u}^c \in \mathbb{R}^N$ is the vector with the numerical approximation of the correction potential on the mesh nodes [23]. In the present work, we utilised linear basis functions $\varphi_i(\mathbf{r})$ ($i = 1, \dots, N$) based on a tetrahedral mesh. In this case, the stiffness matrix \mathbf{K} can be computed without the need of numerical integration schemes [27]. However, numerical quadrature is required for calculating \mathbf{b} , since it depends on the non-linear functions $\nabla u^\infty(\mathbf{r})$. To do so, we used a Gauss-Jacobi integration scheme, usually referred to as the *full subtraction* approach [22]. Simulation of multipolar sources is then achieved by utilising the corresponding expression for the singularity potential.

D. Numerical implementation

We implemented the FE framework in MATLAB 2015a (Natick, MA). As mentioned in Section II-C.2, we computed the source vectors using numerical formulas based on the Gauss-Jacobi method. Quadrature nodes and weights were found using the `jacpts` function from Chebfun [28]. The corresponding integrands were computed analytically using (8) – (10). Additional experiments presented in Section S1 allowed us to select the minimum integration orders needed by each source component to generate negligible errors, which resulted equal to 2, 3, and 5 for monopoles, dipoles, and quadrupoles, respectively. After obtaining the systems of equations, we solved them utilising the preconditioned conjugate gradients method. We used incomplete LU preconditioners and iterated until reaching a tolerance of 10^{-10} . Common average reference was considered in all experiments. Simulations were performed in an Intel i5-4590T CPU @ 2.00GHz with 32Gb RAM.

E. Experimental setup

In a first set of experiments, we tested the accuracy of the FE formulation considering multipolar source models. This was done utilising spherical head representations, for which we derived analytical solutions assuming an anisotropic electrical conductivity field. The second set of experiments illustrates the application of multipolar source models in a realistic scenario, where we highlight their potential for describing extended sources in the macroscale.

1) *Spherical model generation*: We modelled the head as a multi-layered sphere with compartments representing the scalp, skull, cerebrospinal fluid (CSF), and brain. The outer radii were 0.092 m, 0.086 m, 0.08 m, and 0.078 m, respectively. The electrical conductivities were considered isotropic for all compartments, and set to 0.33 S/m, 0.0093 S/m, 1.79 S/m, and 0.33 S/m for the scalp, skull, CSF, and brain layers, respectively. The electric conductivity values were extracted from the relevant literature [21], [29], [30].

We discretised the spherical model using the ISO2Mesh toolbox [31]. Meshes were built to achieve a maximum *radius-edge factor* (defined as the ratio between the radius of the unique circumsphere of a tetrahedron and its shortest edge length) of 1.2. As suggested in [22], we considered a coarser mesh resolution in the brain layer since the volume integral in (13) vanishes in this compartment for sharing the same electrical conductivity as the source neighbourhood. Six models with 39k, 82k, 119k, 281k, 440k, and 640k nodes were generated and utilised in the simulations. A visual representation of these meshes is provided in Section S1.

2) *Analytical solutions*: Assuming a multi-layered spherical head model with piecewise homogeneous and anisotropic conductivity field, the electric potential measured in \mathbf{r} due to a unitary monopole localised in \mathbf{r}_o can be expressed as [24]

$$f(\mathbf{r}_o, \mathbf{r}) = \frac{1}{4\pi} \sum_{n=0}^{\infty} (2n+1) R_n(r_o, r) P_n(\cos \omega_{oe}), \quad (15)$$

where $r_o = |\mathbf{r}_o|$, $r = |\mathbf{r}|$, ω_{oe} is the angle between $\mathbf{r}_o = (x_1, x_2, x_3)$ and \mathbf{r} , $P_n(\cdot)$ is the n th-degree Legendre polynomial, and R_n are functions depending on the media, \mathbf{r}_o , and \mathbf{r} (see [24] for details). To find the potential generated by a multipolar source, we use (15) in (4). In the case of a monopole, the analytical solution becomes $u_m^a(\mathbf{r}_o, \mathbf{r}) = qf(\mathbf{r}_o, \mathbf{r})$. If a dipole is considered, the potential function is given by $u_q^a(\mathbf{r}_o, \mathbf{r}) = \mathbf{q} \cdot \nabla_o f(\mathbf{r}_o, \mathbf{r})$. This expression can be further simplified, leading to [24, eqs. (54)–(58)]

$$4\pi u_q^a(\mathbf{r}_o, \mathbf{r}) = \mathbf{q} \cdot [\hat{\mathbf{r}}_o (S_1 - \cos \omega_{oe} S_0) + \hat{\mathbf{r}} S_0],$$

where

$$S_0 = \frac{1}{r_o} \sum_{n=1}^{\infty} (2n+1) R_n(r_o, r) P_n'(\cos \omega_{oe}),$$

$$S_1 = \sum_{n=1}^{\infty} (2n+1) R_n'(r_o, r) P_n(\cos \omega_{oe}),$$

$\hat{\mathbf{r}}_o \equiv \mathbf{r}_o/r_o = (x_1^o, x_2^o, x_3^o)$, and $\hat{\mathbf{r}} \equiv \mathbf{r}/r = (x_1^e, x_2^e, x_3^e)$. Finally, when considering a quadrupolar source, $u_Q^a(\mathbf{r}_o, \mathbf{r}) = \frac{1}{2} \mathbf{Q} : \nabla_o (\nabla_o f(\mathbf{r}_o, \mathbf{r}))$, for which the terms

$\partial^2 f(\mathbf{r}_o, \mathbf{r}) / \partial x_i \partial x_j$ are needed ($i, j = 1, 2, 3$). These terms can be obtained by adapting [24, eq. (61)] to consider the full quadrupolar moment instead of the dipolar moment. The resulting expression is

$$4\pi \frac{\partial^2 f(\mathbf{r}_o, \mathbf{r})}{\partial x_i \partial x_j} = \frac{S_1}{r_o} (\delta_{ij} - x_i^o x_j^o) + S_2 (x_i^o x_j^o) + \frac{S_0}{r_o} [-(x_j^o x_i^e + x_i^o x_j^e) + (3x_i^o x_j^o - \delta_{ij}) \cos \omega_{oe}] + S_3 [x_i^o (x_j^e - x_j^o \cos \omega_{oe}) + x_j^o (x_i^e - x_i^o \cos \omega_{oe})] + S_4 [(x_i^e - x_i^o \cos \omega_{oe}) (x_j^e - x_j^o \cos \omega_{oe})],$$

where the functions S_i ($i = 2, 3, 4$) are given by

$$S_2 = \frac{1}{r_o} \sum_{n=1}^{\infty} (2n+1) R_n''(r_o, r) P_n(\cos \omega_{oe}),$$

$$S_3 = \frac{1}{r_o} \sum_{n=1}^{\infty} (2n+1) R_n'(r_o, r) P_n'(\cos \omega_{oe}),$$

$$S_4 = \frac{1}{r_o^2} \sum_{n=1}^{\infty} (2n+1) R_n(r_o, r) P_n''(\cos \omega_{oe}).$$

The computation of R_n , P_n , and their corresponding derivatives was done as suggested in [24] (it is noted that the first term in the right-hand side of [24, eq. (65)] should read $(n+1)P_{n-1}' \cos \omega$ instead of $nP_{n-1}' \cos \omega$).

3) *Experiments using spherical models*: Simulations were performed considering monopolar, dipolar, and linear quadrupolar sources in 100 random positions at a distance r_o from the centre, with r_o ranging between $r_{in}/2$ and r_{in} , and r_{in} being the radius of the innermost layer. In the case of monopoles, each simulation consisted in a pair of sources with moments $\pm 10 \mu\text{A}$ and located at a distance r_o from the centre and $2r_o$ between them. In the case of dipoles and quadrupoles, we considered tangentially- and radially-oriented sources with magnitudes 10 nAm and 15 pAm², respectively. These values were selected as population representative moments describing generators of brain activity in the mesoscale [14]. Quadrupolar moments were constructed by tuning the eigenvalues corresponding to the radially/tangentially oriented eigenvectors. For example, for a source located in $(0, 0, 1)$, the corresponding normalised quadrupolar moment for a tangentially oriented source had elements $Q_{11} = 1$, $Q_{12} = 0$, $Q_{13} = 0$, $Q_{22} = -1$, $Q_{23} = 0$, and $Q_{33} = 0$. A total of 162 electrodes uniformly placed on the scalp surface were utilised [32].

We calculated the three standard error measures used in the EEG-FP literature: the relative error (RE), the normalised relative difference measure (RDM), and the magnification factor (MAG). These indices are defined as

$$RE = \frac{\|\mathbf{u}_n - \mathbf{u}_a\|}{\|\mathbf{u}_a\|}, \quad RDM = \left\| \frac{\mathbf{u}_n}{\|\mathbf{u}_n\|} - \frac{\mathbf{u}_a}{\|\mathbf{u}_a\|} \right\|,$$

$$MAG = \left| \frac{\|\mathbf{u}_n\|}{\|\mathbf{u}_a\|} - 1 \right|,$$

where $\|\cdot\|$ stands for the Euclidean norm, and \mathbf{u}_n and \mathbf{u}_a are the vectors representing the numerical and analytical solutions on the sensing positions, respectively. The RE accounts for

general errors in the numerical solution, whereas the RDM and the MAG distinguish between topographic and magnitude errors, respectively. Error-less (i.e. ideal) numerical solutions result in zero values for the three error indices.

In a first experiment, we computed the error measures as a function of the *source eccentricity*, defined as $e = r_o/r_{in}$. Such analysis is standard in the literature, and allows to evaluate the impact of the source position in the simulated potentials.

A second experiment consisted in calculating the RE obtained for eccentric ($e = 0.95$) monopolar, dipolar, and quadrupolar sources as a function of the number of mesh nodes. This analysis is useful for studying the convergence of the numerical method in a worst-case scenario, as well as to determine the minimum conditions under which the results are acceptable [23].

4) *Illustration in a realistic model*: A detailed head model was built based on the Colin 27 high resolution MRI segmentation of the Montreal Neurological Institute [33]. A mesh with 9M tetrahedral elements (1.4M nodes) was created using the ISO2Mesh software as described before. This included the scalp, skull, CSF, and brain compartments, with the same electrical conductivities as in the spherical models. A total of 162 electrodes were placed on the scalp according to the ABC standard (see Section S2 for a visual representation).

The head model was utilised for showing the advantages of equivalent multipoles compared to the standard equivalent dipolar model for describing distributed sources of electrical activity. To this end, we simulated extended sources located on the white matter/grey matter interface, obtained with FreeSurfer [34]. A total of 108 surface points were randomly selected as source centroids, all of them on the left hemisphere. For each of them, we considered four extended sources comprising the surface nodes with geodesic distance to the centroid less or equal than 2.5 mm, 5 mm, 7.5 mm, and 10 mm. This resulted in 432 distributed sources covering an area of 19.6 mm², 78.5 mm², 176.7 mm², and 314.2 mm² (108 each). We used the weighted multiple dipoles (WMD) method with area averaged normals for representing the distributed current density [10], [35]. This method consists in modelling each extended source as the sum of dipoles located in the patch vertices, leading to

$$s(\mathbf{r}) = \sum_{i=1}^{N_s} \mathbf{q}_i \cdot \nabla \delta(\mathbf{r} - \mathbf{r}_i), \quad (16)$$

where N_s is the total number of nodes belonging to the source, and the moments $\mathbf{q}_i = q_i \hat{\mathbf{n}}(\mathbf{r}_i)$ take into account the possibly different size in the triangular elements of the cortical surface tessellation [35]. Using (16) in (6) and (7), we find the equivalent dipolar and quadrupolar moments,

$$\mathbf{q} = \sum_{i=1}^{N_s} \mathbf{q}_i, \quad \mathbf{Q} = \sum_{i=1}^{N_s} (\mathbf{q}_i(\mathbf{r}_i - \mathbf{r}_o)^T + (\mathbf{r}_i - \mathbf{r}_o)\mathbf{q}_i^T).$$

The location \mathbf{r}_o was selected as the closest point to the centroid such that the distance between \mathbf{r}_o and the nearest conductivity change (i.e. the boundary between the brain and CSF compartments) was larger than the distributed source radius. This

was done to comply with the multipolar convergence condition described in Section II-B. Such procedure resulted in lower or equal relative errors than choosing the distributed source centroid (for both dipolar and multipolar source models). The electric potential was then computed for the distributed, dipolar, and multipolar models, and subsequently used to calculate the RE between the solutions obtained with the WMD and both approximations. Finally, we utilised a Mann-Whitney U-test for testing the null hypothesis that the medians of the REs obtained with the equivalent dipolar and multipolar methods were equal.

III. RESULTS

A. Error measures for spherical models

Fig. 1 shows the error measures of the numerical solution of the EEG-FP as a function of the source eccentricity considering monopoles, tangentially-oriented dipoles and linear quadrupoles, and the models composed by 119k and 940k nodes. The advantages of the finer model can be easily appreciated. Equivalent results can be extracted from radially-oriented sources (see Section S1).

In Fig. 2 we present the RE for eccentric ($e = 0.95$) monopolar, dipolar, and quadrupolar sources as a function of the number of nodes in the model discretisation. It can be clearly noted that the subtraction method converges irrespective of the source order.

Additionally, we calculated the time required for computing the source vectors for every head and source models. As expected, the results showed that the computation time depends on the integration order and mesh discretisation, but not on the source model. The time required for calculating each source vector with integration orders equal to 2, 3, and 5 (as described in Section II-D) were 8.83 ± 2.75 s, 11.04 ± 3.26 s, and 47.41 ± 14.36 s, respectively, for the model composed by 119k nodes, and 43.72 ± 15.66 s, 49.08 ± 15.83 s, and 205.05 ± 71.77 s, respectively, for the model with 640k nodes. Further results are presented in Section S1.

B. Illustration in a realistic model

The RE between the potential generated by the distributed sources and the corresponding dipolar and multipolar (i.e. dipole + quadrupole) approximations are presented in Fig. 3. It is noticeable the advantage of the multipolar source representation over the equivalent dipole, which resulted statistically significant for the simulated source extents (i.e. the test rejected the null hypothesis of equal medians at the 0.001% significance level in every case).

In Fig. 4 we show the advantages of the multipolar source approximation over the dipolar model considering an arbitrary distributed source (with area 314.2 mm²) located on the frontal lobe. The difference in the topographical error is noteworthy.

IV. DISCUSSION

The framework presented here provides scientists with a computational resource to simulate electromagnetic signals

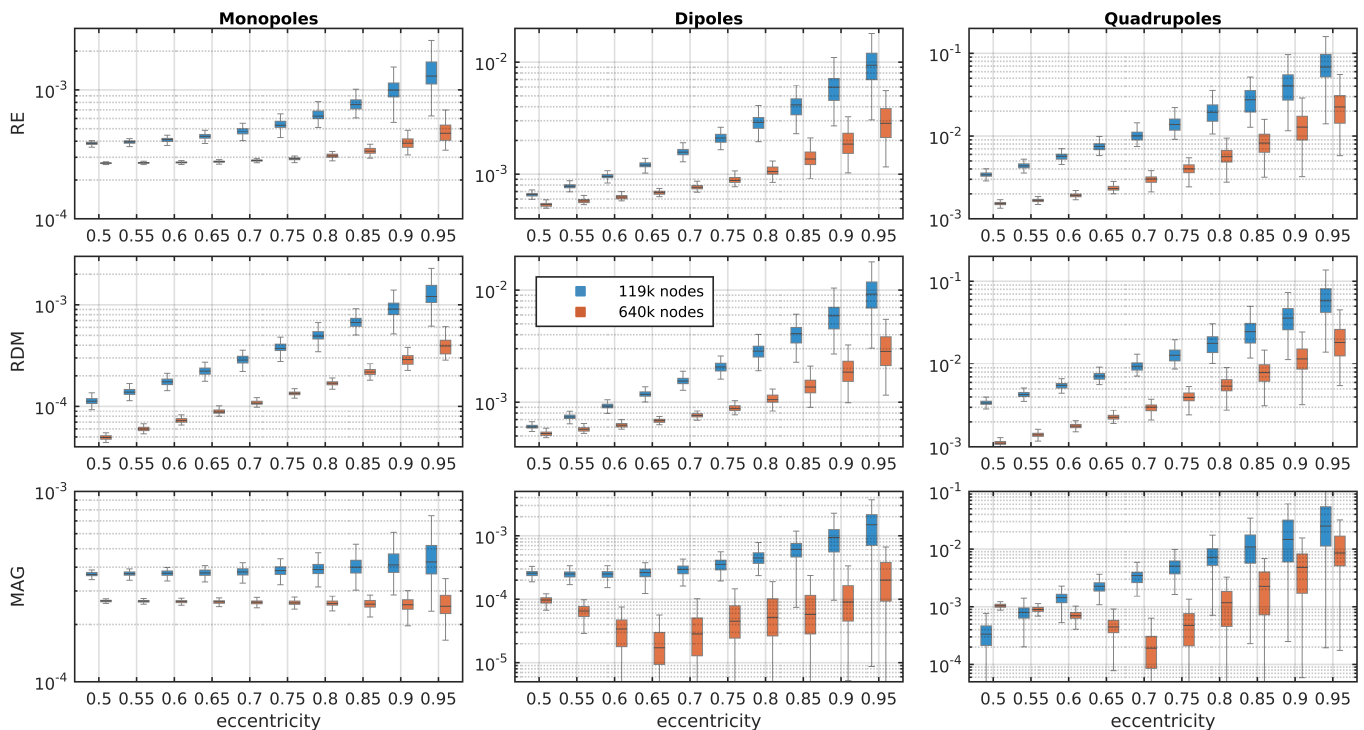


Fig. 1. Error measures for the numerical solutions of the EEG-FP as a function of the source eccentricity. Results corresponding to monopoles, tangential dipoles, and tangential linear quadrupoles are depicted in different columns. RE, RDM, and MAG are shown in different rows. Simulations based on models with 119k and 640k nodes are presented in different colours.

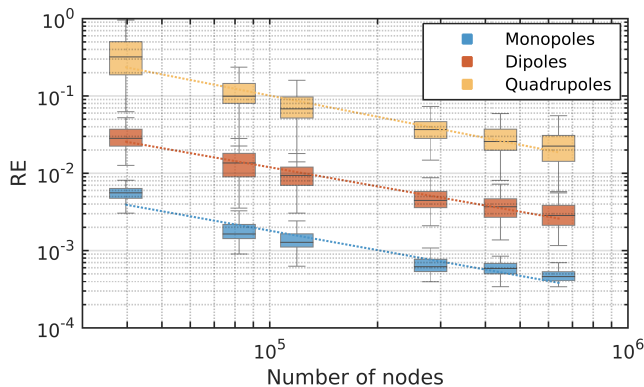


Fig. 2. RE of the solution of the EEG-FP as a function of the number of nodes utilised in the simulations. Results are presented for monopoles, tangential dipoles, and tangential linear quadrupoles with eccentricity $e = 0.95$. Power-law fitting functions are also shown with dotted lines (i.e. $RE \propto n^\alpha$, with n being the number of nodes, and $\alpha = -0.83, -0.82, -0.91$ for monopolar, dipolar, and quadrupolar sources, respectively).

generated by monopoles, dipoles, and quadrupoles in realistic head models, i.e. comprising non-spherical tissue layers and heterogeneous and anisotropic electrical conductivity fields. This enables researchers, for the first time, to test the usefulness of multipolar source components in personalised head models, which are acknowledged for being crucial in EEG (either invasive [36] or non-invasive [19], [20], [37]–[39]) and MEG [19], [40], [41] source characterisation. The adoption of multipolar sources allows not only to refine phenomenological representations of brain activity, as those presented in Section III-B, but also to relate acquisitions with

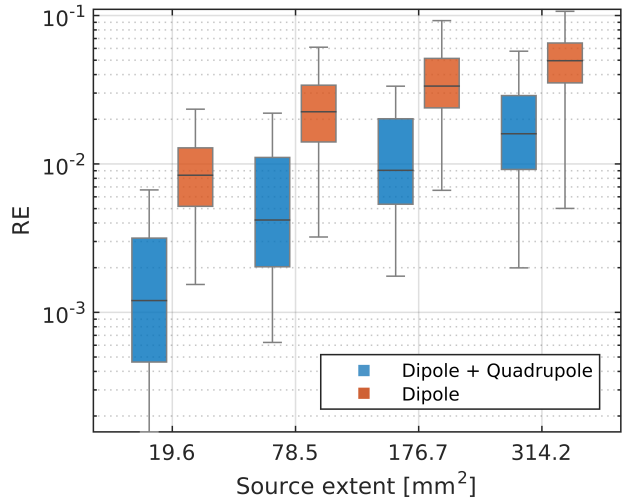


Fig. 3. RE between the potential generated by a distributed source and the equivalent dipolar (orange) and multipolar (blue) approximations as a function of the source extent. The difference between errors is statistically significant for all source extents (i.e. the test rejected the null hypothesis of equal medians at the 0.001% significance level in every case).

biophysically-rooted parameters in the mesoscale [14]. This makes multipolar models a prospective tool to be used to gain mechanistic insights into signal generation, and therefore worth attention.

Besides the numerical framework, we derived analytical solutions of the EEG-FP for multipolar current sources in

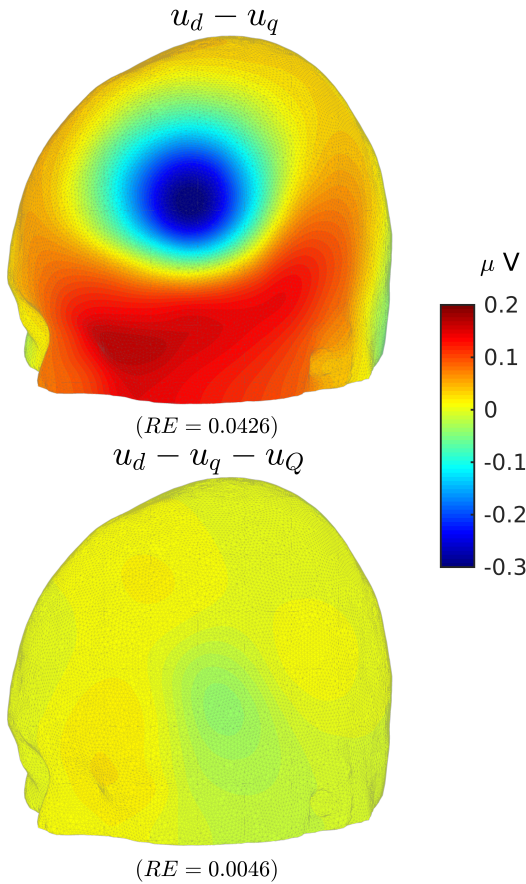


Fig. 4. Difference between the electric potential due to a distributed source with area 314.2 mm^2 and the dipolar (top) and multipolar (bottom) approximations. The presented errors correspond to a RE of 0.0426 in case of considering the dipolar model, and 0.0046 if the multipolar representation is used.

multi-layered spherical head models with anisotropic electrical conductivity field. In particular, we obtained analytical expressions for the electric potential distribution due to quadrupolar sources, complementing the results for monopolar and dipolar components derived by de Munck and Peters [24]. Analytical formulas have a crucial role in the development of numerical techniques, providing a means to benchmark results and compare between methods (e.g. [42]). In this context, the results from Section II-E.2 provide a valuable resource for advancing in the development of numerical algorithms to better describe generators of brain activity and the electromagnetic field they generate. Moreover, they can be used to extend and refine other existing numerical approaches for solving the EEG-FP based on analytical expressions, such as the Locally Spherical Model with Anatomical Constraints technique [43].

Experiments performed in spherical head models allowed to understand the computational requirements for simulating multipolar sources. Fig. 1 shows that error measures increase with the source eccentricity, as previously reported for dipoles [22]. Such pattern was found more pronounced as the order of the multipolar component became larger. Moreover, error measures were found to increase with the order of the

source component. This phenomenon was further confirmed in Fig. 2, where the RE obtained for eccentric quadrupoles resulted approximately one order of magnitude larger than that corresponding to dipoles for almost any mesh discretisation. This evidence suggests that the simulation of quadrupolar components would require a much finer tessellation than that needed by dipolar sources for achieving a given RE. Nevertheless, head models with more than 1.3M nodes are increasingly adopted (e.g. [23], [44], as well as in this study), leading to maximum REs lower than 10^{-2} for any source model and eccentricity. Such errors can be assumed to have relatively little impact on source localisation (less than 5 mm for dipolar sources [30]).

Using a realistic head model, we showed that the inclusion of quadrupolar components to the standard equivalent dipolar source representation benefits the description of extended current generators. Results displayed in Fig. 3 show that the multipolar expansion provides statistically significant improvements in the EEG-FP over standard equivalent dipolar models regardless of the source extent. In the case of sources with an area equal to 314.2 mm^2 , the incorporation of the quadrupolar term was found to reduce the average error five times to achieve an RE of approximately 10^{-2} , which may become noticeable in the estimated source parameters. This improvement is expected to be even more noticeable in intracortical studies, where higher signal-to-noise ratios would allow a detailed description of the mesoscopic nature of generators of brain activity.

Multipolar source models are expected to have a major impact in the solution of the E/MEG inverse problem (IP). In this direction, several approaches have been presented in the MEG literature exploiting the availability of analytical formulas for spherical head models [10], [45], [46]. Using a single shell spherical head representation, Jerbi *et al.* showed that source estimation errors were consistently lowered by the addition of the quadrupolar term to the standard dipole [10]. Extrapolating these results to the present study, the lower REs obtained with the incorporation of the quadrupolar component (Fig. 3) would indicate an increased accuracy in the range 0.5–5 mm when compared to the standard dipole model (see Section S2). However, the aforementioned E/MEG-IP methods rely on computational simplicities that are not available if personalised head models are adopted. In this case, algorithms based on the lead-field matrix must be used [7]. If dipolar components are considered, the lead-field matrix will depend on the source location and moment, which are properly described by six parameters (three for the source location, and three for the dipolar moment). This number increases to eight if quadrupolar sources are assumed, forcing scientists to redesign EEG-IP strategies. We are currently working in the extension of E/MEG-IP algorithms to include multipolar components, and test their efficiency based on real acquisitions.

In addition to enhancing source localisation results, multipolar source models have the potential to provide more reliable links between macroscopic measurements and parameters describing cellular and circuit level neural generators. One of the most prominent frameworks allowing such connection is the Human Neocortical Neurosolver (HNN) [47], which has

proven its usefulness in the mesoscopic description of beta and mu rhythms [15], [48], [49]. The HNN relies on a mathematical model linking parameters at the column level (such as ionic currents) with the equivalent current dipole as estimated with E/MEG [15]. As mentioned before, multipolar models mitigate source modelling errors introduced by the equivalent dipole, increasing the accuracy of the lead-field matrices with the potential of providing better equivalent source estimates. For this reason, we expect that the incorporation of multipolar source components to the HNN will contribute to further improve the robustness of the estimated mesoscopic parameters, as well as to facilitate the incorporation of other complementary information, such as the spatio-temporal potential profile [14].

It is important to note that in this work, as in most papers dedicated to solve the EEG-FP, we focused our attention on reducing the errors between the analytical and numerical solutions in spherical head models. More explicitly, we aimed at minimising error measures such as the RE, RDM, and MAG. Although these metrics are important for characterising the fidelity of the simulated potentials, their relation with the accuracy in the EEG-IP is not fully understood. It is known that there exist many sources of noise impacting in the EEG-IP, such as the thermal noise [50], the electrical conductivity [27], the geometry [51], the location of the electrodes [52], and, most importantly, the background activity [53], [54]. This suggests that extremely accurate solutions of the EEG-FP may not be fully exploited due to inevitable uncertainties in the overall analysis. We are currently performing a thorough study on the usefulness of the standard error measures in the context of the EEG-IP.

From a theoretical perspective, the methodology introduced allows to guarantee the existence and uniqueness of the solution for balanced source models, e.g. a pair of monopoles with opposite moment, dipoles, and quadrupoles. Moreover, the subtraction approach appears as the most appropriate method for solving the EEG-FP considering quadrupolar sources, as it allows the use of linear basis functions without needing a denser mesh discretisation near the source position. This will not be the case if the partial integration [55] or Venant [56] methods are adopted, which are expected to require a finer mesh density close to the source location for achieving similar error measures. In the particular case of the partial integration approach, it will also require the use of quadratic basis functions for computing the second order derivatives, making its computational cost even higher.

From a practical point of view, the full subtraction technique presents two major weaknesses compared to others. First, it requires more processing time for the computation of the source vector than other competing methods, limiting its usability in clinical settings. Second, it may introduce *skull leakage effects* in areas where the thickness of the skull is in the range of the mesh resolution, forcing the user to generate accurate and refined discretisations in the CSF and skull layers [57]. We are now working in some alternatives to solve these limitations. With regard to the first point, we are extending the analytical subtraction approach recently introduced for dipolar source models to multipoles [58]. This consists in obtaining exact expressions for the element source vectors by

means of the application of Gauss theorems, avoiding time-consuming numerical integration schemes while increasing the accuracy of the results. For the second point, we plan to test the multipolar source models using the discontinuous Galerkin framework, which was shown to minimise leakage effects without the need of extra mesh refinements [57].

V. CONCLUSIONS

We have presented a numerical method to simulate the electric potential distribution due to multipolar current generators in realistic head models. The framework is based on the full subtraction FE approach, which is known for being accurate and theoretically rigorous. Using spherical head models, we demonstrated that the methodology leads to very small errors in the EEG-FP for the mesh discretisations generally adopted in the field. We illustrated the application of the method in the description of extended sources of brain activity, for which we showed that the incorporation of multipolar components reduces the relative error between five and ten times compared to a single dipole. Moreover, these sources have the potential to provide a link between macroscopic acquisitions (such as E/MEG) and biophysical parameters defining the source at smaller scales. The MATLAB implementation of the framework (including the analytical solutions derived in Section II-E.2) is publicly available through the FEMEG toolbox (<https://femeg.github.io>).

ACKNOWLEDGEMENTS

The author thanks Dr. Nicolás von Ellenrieder and Prof. Carlos H. Muravchik for inspiring discussions.

REFERENCES

- [1] H. Berger, "Über das Elektroenkephalogramm des Menschen," *Arch Psychiatr Nervenkr*, vol. 87, pp. 527–570, 1929.
- [2] E. Adrian and B. Matthews, "The Berger rhythm: potential changes from the occipital lobes in man," *Brain*, vol. 57, pp. 355–385, 1934.
- [3] J. Shaw and M. Roth, "Potential distribution analysis. II: A theoretical consideration of its significance in terms of electric field theory," *Electroencephalogr Clin Neurophysiol*, vol. 7, pp. 285–292, 1955.
- [4] Y. Okada *et al.*, "Genesis of magnetic signals in a mammalian CNS structure," *Electroencephalogr Clin Neurophysiol.*, vol. 103, pp. 474–85, 1997.
- [5] J. de Munck *et al.*, "Mathematical dipoles are adequate to describe realistic generators of human brain activity," *IEEE Trans Biomed Eng.*, vol. 35, no. 11, pp. 960–966, 1988.
- [6] M. Hamalainen *et al.*, "Magnetoencephalography theory, instrumentation, and applications to noninvasive studies of the working human brain," *Rev Mod Phys.*, vol. 65, no. 2, pp. 413–497, 1993.
- [7] S. Baillet *et al.*, "Electromagnetic brain mapping," *IEEE Signal processing magazine*, vol. 18, no. 6, pp. 14–30, 2001.
- [8] J. Haueisen *et al.*, "On the Influence of Volume Currents and Extended Sources on Neuromagnetic Fields: A Simulation Study," *Ann Biomed Eng.*, vol. 23, pp. 728–39, 1995.
- [9] A. Hillebrand and G. Barnes, "A quantitative assessment of the sensitivity of whole-head MEG to activity in the adult human cortex," *Neuroimage*, vol. 16, pp. 638–50, 2002.
- [10] K. Jerbi *et al.*, "Localization of realistic cortical activity in MEG using current multipoles," *Neuroimage*, vol. 22, pp. 779–593, 2004.
- [11] Z.-L. Lü and S. Williamson, "Spatial extent of coherent sensory-evoked cortical activity," *Exp. Brain Res.*, vol. 84, pp. 411–416, 1991.
- [12] N. von Ellenrieder *et al.*, "Extent of cortical generators visible on the scalp: Effect of a subdural grid," *Neuroimage*, vol. 101, pp. 787–795, 2014.

- [13] J. Milstein and C. Koch, "Dynamic moment analysis of the Extracellular Electric Field of a Biologically Realistic Spiking Neuron," *Neural Comput*, vol. 20, pp. 2070–2084, 2008.
- [14] J. Riera *et al.*, "Pitfalls in the dipolar model for the neocortical EEG sources," *J Neurophysiol.*, vol. 108, no. 4, pp. 956–975, Aug. 2012.
- [15] M. Sherman *et al.*, "Neural mechanisms of transient neocortical beta rhythms: converging evidence from humans, computational modeling, monkeys, and mice," *PNAS*, vol. 113, pp. E4885–E4894, 2016.
- [16] J. Stratton, *Electromagnetic Theory*. McGraw-Hill, USA, 1941.
- [17] G. Nolte and G. Curio, "On the Calculation of Magnetic Fields Based on Multipole Modeling of Focal Biological Current Sources," *Biophys J.*, vol. 73, pp. 1253–1262, 1997.
- [18] K. Jerbi *et al.*, "On MEG forward modelling using multipolar expansions," *Phys Med Biol.*, vol. 47, pp. 523–555, 2002.
- [19] B. Cuffin, "Effects of Head Shape on EEGs and MEGs," *IEEE Trans Biomed Eng.*, vol. 37, no. 1, pp. 44–52, 1990.
- [20] L. Beltrachini *et al.*, "Impact of head models in N170 component source imaging: results in control subjects and ADHD patients," *J Phys Conf Series*, vol. 332, no. 1, p. 972060, 2011.
- [21] C. Ramon *et al.*, "Influence of head models on EEG simulations and inverse source localizations," *Biomed Eng Online*, vol. 5, p. 10, 2006.
- [22] F. Drechsler *et al.*, "A full subtraction approach for finite element method based source analysis using constrained Delaunay tetrahedralisation," *Neuroimage*, vol. 46, pp. 1055–1065, 2009.
- [23] L. Beltrachini, "Sensitivity of the projected subtraction approach to mesh degeneracies and its impact on the forward problem in EEG," *IEEE Trans Biomed Eng.*, 2018, in press.
- [24] J. de Munck and M. Peters, "A fast method to compute the potential in the multisphere model," *IEEE Trans Biomed Eng.*, vol. 40, no. 11, pp. 1166–1174, 1993.
- [25] J. Malmivuo and R. Plonsey, *Bioelectromagnetism - Principles and Applications of Bioelectric and Biomagnetic Fields*. Oxford University Press, New York, 1995.
- [26] C. Wolters *et al.*, "Numerical Mathematics of the Subtraction Method for the Modeling of a Current Dipole in EEG Source Reconstruction Using Finite Element Head Models," *SIAM J Sci Comput.*, vol. 30, no. 1, pp. 24–45, 2007.
- [27] M. Fernández-Corazza *et al.*, "Analysis of parametric estimation of head tissue conductivities using Electrical Impedance Tomography," *Biomed. Signal Process. Control*, vol. 8, no. 6, pp. 830–837, 2013.
- [28] T. Driscoll *et al.*, *Chebfun Guide*. Pafnuty Publications, Oxford, UK, 2014.
- [29] S. Baumann *et al.*, "The electrical conductivity of human cerebrospinal fluid at body temperature," *IEEE Transactions on Biomedical Engineering*, vol. 44, no. 3, pp. 20–23, 1997.
- [30] M. Dannhauer *et al.*, "Modeling of the human skull in EEG source analysis," *Human Brain Mapping*, vol. 32, pp. 1383–1399, 2011.
- [31] Q. Fang and D. Boas, "Tetrahedral mesh generation from volumetric binary and gray-scale images," in *Proc. IEEE Intl. Symp. Biomed. Imaging*, 2009, pp. 1142–1145.
- [32] C. Koay, "Analytically exact spiral scheme for generating uniformly distributed points on the unit sphere," *J Comput Sci.*, vol. 2, pp. 88–91, 2011.
- [33] B. Aubert-Broche *et al.*, "A new improved version of the realistic digital brain phantom," *NeuroImage*, vol. 32, no. 1, pp. 138–145, 2006.
- [34] A. Dale *et al.*, "Cortical Surface-Based Analysis I: Segmentation and Surface Reconstruction," *Neuroimage*, vol. 9, pp. 179–194, 1999.
- [35] N. von Ellenrieder *et al.*, "On the EEG/MEG forward problem solution for distributed cortical sources," *Med Biol Eng Comput*, vol. 47, pp. 1083–91, 2009.
- [36] —, "Electrode and brain modeling in stereo-EEG," *Clin. Neurophysiol.*, vol. 123, pp. 1745–1754, 2012.
- [37] G. Huiskamp *et al.*, "The need for correct realistic geometry in the inverse EEG problem," *IEEE Trans Biomed Eng.*, vol. 46, no. 11, pp. 1281–1287, 1999.
- [38] B. Vanrumste *et al.*, "Comparison of performance of spherical and realistic head models in dipole localization from noisy EEG," *Med Eng Phys.*, vol. 24, no. 6, pp. 403–418, 2002.
- [39] F. Vatta *et al.*, "Realistic and Spherical Head Modeling for EEG Forward Problem Solution: A Comparative Cortex-Based Analysis," *Comput Intell Neurosci.*, p. 972060, 2010.
- [40] R. Van Uiter and C. Johnson, "Can a Spherical Model Substitute for a Realistic Head Model in Forward and Inverse MEG Simulations?" in *Proc 13th Intl Conf Biomag.*, 2002, pp. 798–800.
- [41] M. Stenroos *et al.*, "Comparison of three-shell and simplified volume conductor models in magnetoencephalography," *Neuroimage*, vol. 94, pp. 337–48, 2014.
- [42] J. Vorwerk *et al.*, "Comparison of boundary element and finite element approaches to the EEG forward problem," *Biomedizinische Technik*, vol. 57, pp. 795–798, 2012.
- [43] D. Brunet *et al.*, "Spatiotemporal analysis of multichannel EEG: CAR-TOOL," *Comput Intell Neurosci.*, p. 813870, 2011.
- [44] L. Fiederer *et al.*, "The role of blood vessels in high-resolution volume conductor head modeling of EEG," *Neuroimage*, vol. 128, pp. 193–208, 2016.
- [45] J. C. Mosher *et al.*, "MEG source imaging using multipolar expansions," in *Lecture notes on computer science 1613*, 1999, pp. 15–28.
- [46] T. Nara, "Algebraic Reconstruction of Current Dipoles and Quadrupoles in Three-Dimensional Space," *Math Probl Eng.*, vol. ID 413980, 2013.
- [47] [Online]. Available: <https://hnn.brown.edu>
- [48] S. Jones *et al.*, "Neural correlates of tactile detection: a combined magnetoencephalography and biophysically based computational modeling study," *J Neurosci.*, vol. 27, pp. 10751–10764, 2007.
- [49] —, "Quantitative analysis and biophysically realistic neural modeling of the MEG mu rhythm: rhythmogenesis and modulation of sensory-evoked responses," *J Neurophysiol.*, vol. 102, pp. 3554–3572, 2009.
- [50] C. Muravchik and A. Nehorai, "EEG/MEG error bounds for a static dipole source with a realistic head model," *IEEE Trans Signal Process.*, vol. 49, pp. 470–484, 2001.
- [51] N. von Ellenrieder *et al.*, "Effect of Geometric Head Model Perturbations on the EEG Inverse Problem," *IEEE Trans. Biomed. Eng.*, vol. 53, pp. 421–429, 2005.
- [52] L. Beltrachini *et al.*, "General bounds for electrode mislocation on the EEG inverse problem," *Comput. Methods Programs Biomed.*, vol. 103, no. 1, pp. 1–9, 2011.
- [53] J. de Munck *et al.*, "A random dipole model for spontaneous brain activity," *IEEE Trans Biomed Eng.*, vol. 39, no. 8, pp. 791–804, 1992.
- [54] L. Beltrachini *et al.*, "Shrinkage Approach for Spatiotemporal EEG Covariance Matrix Estimation," *IEEE Trans Signal Process.*, vol. 61, no. 7, pp. 1797–1808, 2013.
- [55] D. Weinstein *et al.*, "Lead-field bases for electroencephalography source imaging," *Ann Biomed Eng.*, vol. 28, pp. 1059–1066, 2000.
- [56] H. Buchner *et al.*, "Inverse Localization of Electric Dipole Current Sources in Finite Element Models of the Human Head," *Electroenc Clin Neurophysiol.*, vol. 102, pp. 267–278, 1997.
- [57] C. Engwer *et al.*, "A discontinuous galerkin method to solve the eeg forward problem using the subtraction approach," *SIAM J Sci Comput.*, vol. 39, pp. B138–B164, 2017.
- [58] L. Beltrachini, "The analytical subtraction approach for solving the forward problems in E/MEG," in *Proc 21st Intl Conf Biomagnetism (BIOMAG)*, 2018, pp. Abstract M–074.